International Journal of
INTELLIGENT SYSTEMS AND APPLICATIONS IN ENGINEERING
ISSN:2147-6799 www.ijisae.org Original Research Paper

Advanced Fetal Cardiac Anomaly Diagnosis with Multispectral LBP Transformation Techniques and Deep Learning Models

Divya M. O.[1], M. S. VIjaya[2]

Submitted: 15/01/2024 **Revised**: 23/02/2024 **Accepted**: 01/03/2024

Abstract: This research is dedicated to developing an advanced deep learning diagnostic model capable of accurately diagnosing fetal cardiac anomalies in real-time ultrasound scan images. To achieve this, the dataset utilized in the previous research has undergone a transformation using Multispectral Local Binary Pattern (MLBP) and Adaptive Multispectral Local Binary Pattern (AMLBP) techniques. Local Binary Pattern (LBP) is an essential texture image feature, and MLBP and AMLBP are enhanced versions designed to capture intricate local structures and patterns within each image. Unlike the traditional LBP transformation, MLBP and AMLBP take color channels into account, allowing for more comprehensive feature extraction from the input images. The previously formed FetalEcho_V05 dataset has been transformed into two distinct datasets: FetalEcho_V0502 using MLBP and FetalEcho_V0503 using AMLBP. Both of these datasets are then employed in training customized versions of AlexNet, custom CNN(CCNN), VGG16, and ResNet50 deep learning (DL) models to create powerful classifiers. Among all the models, CCNN model demonstrated the best performance on the FetalEcho_V0503 dataset, showcasing its superiority in accurately diagnosing fetal cardiac anomalies from real-time ultrasound scan images.

Keywords: *Deep learning, Diagnosis, Fetal cardiac anomaly, Image transformation, Local Binary Pattern, Multispectral*

1. Introduction

Congenital heart defect (CHD) in fetuses refers to structural abnormalities or malformations in the heart that are present at birth. These are conditions that occur while the baby's heart is developing during pregnancy. Such abnormalities can involve issues with the heart's chambers, valves, blood vessels, or other structural components. These anomalies may vary in severity and can have a significant impact on the baby's health and well-being. Accurate diagnosis and understanding of fetal cardiac structural abnormalities are crucial for appropriate medical management and intervention both during pregnancy and after birth. Diagnosing and studying these anomalies often involve the use of ultrasound and other diagnostic techniques to assess the fetal heart's structure and function. Researchers and medical professionals often study these conditions to improve their detection, treatment, and management, ultimately aiming to ensure the best possible outcomes for affected infants. These defects can affect the walls, valves, or blood vessels of the heart, disrupting its normal functioning. CHD can vary in severity, ranging from minor issues that may not require treatment to complex conditions that necessitate immediate medical intervention. Prenatal detection and diagnosis of CHD are crucial as they allow for early interventions and appropriate management plans to be put in place, improving outcomes for affected infants. Various diagnostic techniques, including ultrasound imaging and fetal echocardiography, are used to identify CHD in the fetus, enabling timely medical interventions and specialized care during and after birth. Early detection and intervention can significantly impact the prognosis and quality of life for infants with CHD.

The current process of diagnosing fetal heart anomalies involves a combination of prenatal screening tests, fetal ultrasound imaging, and specialized examinations. Prenatal screening tests, such as maternal blood tests and non-invasive prenatal testing, help identify potential risk factors and indicate the need for further diagnostic evaluations. Fetal ultrasound imaging plays a crucial role in visualizing the fetal heart and detecting any structural abnormalities or functional impairments. These ultrasound scans are typically performed by skilled sonographers or obstetricians and involve a detailed assessment of the fetal heart's chambers, valves, blood flow patterns, and overall cardiac function. The findings from these diagnostic tests are then interpreted by specialized fetal cardiologists or pediatric cardiologists, who provide an accurate diagnosis and guide subsequent management and treatment plans. The current process of

[1*]*Department of Computer Science, PSGR Krishnammal College for Women, Coimbatore, Tamilnadu, India*
[2]*Department of Computer Science, PSGR Krishnammal College for Women, Coimbatore, , Tamilnadu, India*
divyammo@gmail.com
**Corresponding Author: Divya M O*
**Department of Computer Science, PSGR Krishnammal College for Women, Coimbatore, Tamilnadu, India*
*[0000-0003-1983-7364]1**
[0000-0002-4623-5572]2

diagnosing fetal heart anomalies combines medical expertise, advanced imaging technologies, and specialized evaluations to ensure early detection and appropriate care for affected infants.

The manual system for early diagnosis of fetal congenital heart defects (CHD) is associated with several drawbacks. One limitation is the subjectivity involved, as interpretations of fetal heart images can vary among healthcare professionals, leading to inconsistent and potentially incorrect diagnoses. Additionally, manual analysis can be time-consuming, requiring significant effort from practitioners and potentially causing delays in diagnosis and subsequent treatment planning. Interobserver variability further contributes to inconsistencies in diagnostic outcomes, particularly in regions with limited access to specialized expertise. Furthermore, manual diagnosis lacks automation and does not leverage advanced technologies such as artificial intelligence and machine learning. Overcoming these limitations is crucial for improving early detection of fetal CHD.

There are statistics that indicate a relatively poor diagnosis rate of fetal heart anomalies. These statistics highlight the challenges and limitations in accurately identifying and diagnosing these conditions during prenatal care. According to some studies, the detection rate of major fetal heart anomalies during routine prenatal ultrasound screenings ranges from approximately 30% to 50%. This means that a significant number of cases may go undetected or be misdiagnosed, leading to delayed or inadequate management of these conditions. The reasons for the lower detection rate can vary and may include factors such as the complexity of cardiac abnormalities, limitations of imaging techniques, variations in operator expertise, and the timing of ultrasound examinations. Furthermore, certain cardiac defects may be more challenging to visualize and diagnose, requiring specialized expertise and advanced imaging modalities. These statistics emphasize the need for ongoing research, advancements in imaging technology, and improved training and collaboration among healthcare professionals involved in prenatal care to enhance the early detection and accurate diagnosis of fetal heart anomalies.

The development and implementation of automated and computer-aided diagnostic systems have the potential to enhance accuracy, efficiency, and consistency in fetal CHD diagnosis, ultimately improving patient outcomes. Hence it is vital and need of the hour to develop an automated ststem for capturing real-time images and diagnose the fetal cardiac anomaly.

2. Literature Review

A literature review is conducted for understanding the scope of LocalBinaryPatterns for analysing medical images, class wise evaluation of performance of AI models and to establish the scope of the research. The following research had implemented the same concept in a similar domain and proved to be successful.

[1] Patil et al. concentrate on emotion recognition, which is pivotal in human cognition, innovation, and creativity. Real-time emotion detection encounters challenges like noise and hardware limitations. To tackle this, the researchers propose a hardware setup comprising an ECG sensor, a temperature sensor, and a signal processing circuit. ECG data is utilized to compute RR intervals, and machine learning techniques are employed to predict emotions using these features. Emotions are displayed on the Arduino serial port, leveraging the WESAD benchmark dataset and various libraries. The paper introduces several innovative aspects, including ECG utilization for emotion detection, real-time temperature and ECG data capture, real-time emotion visualization on the Arduino serial port, and performance evaluation using F1 score, macro average, and weighted average. It also compares the performance of different algorithms, emphasizing the superiority of probability-based Naive Bayes over traditional methods like KNN, SVM, and Random Forest. The article presents performance metrics through interactive computations, tabular representation, and graphical display.

Khasendar et al. [2] aim to develop and validate a computerized model for classifying malignant or banign ovarian masses using ultrasound images. The images undergo pre-processing and enhancement, and LBP Histograms are extracted. A SVM is trained and achieved with accuracy of 0.62 for the original images, which significantly improves to 0.77 when the images when pre-processed and treated with a LBP operator. This study demonstrates the effectiveness of SVM in accurately categorizing ovarian masses and underscores the importance of incorporating texture-related features for enhanced classification.

Nanni et al. [3] explore the application of image-based machine learning techniques, specifically focusing on various Local Binary Patterns (LBP) as texture descriptors in medical image analysis. The paper provides an extensive literature review of existing LBP variants, discussing their strengths and weaknesses. Additionally, the authors conduct new experiments using different LBP-based descriptors and propose novel texture descriptors specifically designed for biomedical images. These descriptors capture texture information by considering different neighborhood calculation shapes and grayscale difference encodings. The extracted

features are then utilized to train SVM classifier. The study aims to enhance the understanding of LBP variants and their effectiveness in biomedical image analysis, contributing to the advancement of medical imaging techniques.

Zeebaree et al. [4] introduce a feature-based fusion scheme for breast cancer image pattern recognition. By enhancing Local Binary Pattern (LBP) features and utilizing filtered noise reduction, the proposed method achieves high accuracy, sensitivity, and specificity. The multi-level fusion scheme generates diverse features from pre-processed ultrasound images, leading to improved classification results. The approach shows great potential for enhancing breast cancer image recognition and improving the accuracy of diagnosis.

In a meta-analysis by Holland et al. [12], the impact of prenatal versus postnatal diagnosis of cardiac anomalies on mortality rate is examined. The results underscore the importance of prenatal diagnosis in reducing postnatal mortality associated with congenital heart defects (CHDs).

Suard et al. [13] conduct an observational study to evaluate the accurateness of prenatal diagnosis of CHDs in the South France. This study, encompassed 249,070 deliveries, finds that the diagnosis-rate for Group-1 CHDs (non-repairable anomalies) was 97.8%, while Group-2 (anatomically repairable with neonatal cardiologic attention) had a diagnosis rate of 6.3%, and Group-3(no alternative anatomical process required) had a diagnosis rate of 65.9%. The findings suggest the need for improved prenatal and postnatal diagnosis for better management of Group 2 and Group 3 CHDs.

Changlani et al. [14] examine the shortterm outcomes in infants with prenatal-diagnosis of CHDs in a tertiary cardiovascular attention centre. The study, including 552 fetuses diagnosed with CHDs, demonstrates that prenatal identification of CHDs facilitated planned delivery in a specialized cardiac care centre, resulting in favorable outcomes, especially among individuals receiving devoted postnatal cardiac attention.

Vijayaraghavan et al. [15] conduct an experimental study to compare the consequences of prenatal and postnatal-diagnosis of CHDs, particularly focusing on the concept of prearranged peripartum care in low to middle income countries. This study highlights the need for better implementation of prearranged care for neonates with critical congenital heart defects in resource-constrained settings.

The previous research strongly established the need of the implementation even then there are no published implementations available for the same. The research explores the possibilities, the development and integration of real-time automated diagnostic systems into fetal congenital heart disease (CHD) diagnosis with the help of texture feature based image transformations. By harnessing the power of technology, these systems can amplify accuracy, streamline processes, and foster consistency in the diagnosis of fetal CHD.

3. Data Collection and Preprocessing

The FetalEcho_V05 dataset was developed in the previous research which is an integral part of a comprehensive research work on identifying structural heart defects in developing fetuses. The dataset consists of 1600 images obtained from esteemed sources such as specialized fetal clinics, renowned clinical experts, and reputable research repositories like Radiopedia and Fetal Medicine foundations. Every image underwent rigorous manual classification and validation by clinical specialists. It includes 16 distinct classes representing critical structural anomalies such as Atrial Septal Defect, Ventricular Septal Defect, and Tetralogy of Fallot, as well as normal images. To maintain accuracy and reliability, the dataset was carefully balanced and standardized, with all images adjusted to a consistent resolution of 256 * 256 * 3. To ensure exceptional quality, data collection involved sourcing from esteemed establishments, including specialized fetal clinics, renowned clinical experts, and active forums in fetal medicine. These stringent measures guarantee the dataset's credibility and make it a valuable resource for in-depth studies and advanced analyses of structural heart defects in developing fetuses.

Extensive research focused on optimizing pre-processing techniques were done for the FetalEcho_V05 dataset, aiming to unlock its true potential. Rescaling, normalization, and filtering emerged as key techniques for enhancing the dataset. Rescaling ensured uniformity by resizing images to a fixed size. Normalization tackled brightness and contrast variations, improving robustness. Filtering eliminated noise, blurriness, and enhanced image details. Evaluating different preprocessing techniques using AlexNet, noise removal achieved 87% accuracy, blur removal contributed in improving it to 88%, and the sharpening yielded 69%. The combination of blur and noise removal reached an impressive 89% accuracy. The combination of Noice removal and Sharpening demonstrated 57% accuracy and Blur removal and sharpening showcased 77% accuracy. For this series of experiments the dataset versions were created from the base dataset named FetalEcho. The versions were numbered from FetalEcho_V01 to FetalEcho_V08. The FetalEcho_V05 dataset was the one which underwent the Blur removal and Noice removal Preprocessing. Based on these findings, the successful

pre-processing methodology was identified and the FetalEcho_V05 dataset selected for further experiments.

Fig.1 shows some sample images from FetalEcho_V05 dataset.

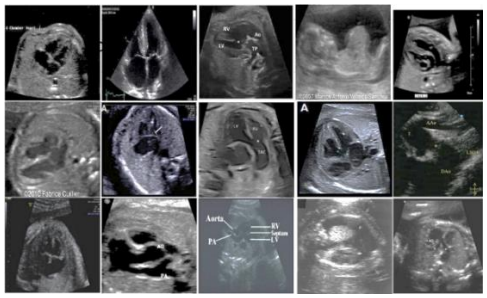

Fig.1 Sample images from FetalEcho_V05

4. Methodology

The Local Binary Pattern (LBP) serves as a highly utilized texture descriptor within computer vision and image analysis, holding significant importance across numerous classification endeavors. LBP is highly robust to changes in illumination, making it effective in scenarios where lighting conditions can vary. It encodes local texture patterns, making it insensitive to overall brightness changes. LBP effectively captures texture information by considering the relationships between a pixel and its neighbouring pixels. This is particularly valuable in tasks where texture plays a significant role, such as texture classification or material recognition. It is computationally efficient and simple to implement. It involves binary comparisons of pixel values, making it suitable for real-time or resource-constrained applications. It can be modified to achieve rotation invariance, which is important in scenarios where the orientation of the texture patterns may vary. This makes it suitable for a widespread variety of applications. It is robust to noise to some extent, as it focuses on the relationships between pixels in a local neighbourhood. This can be particularly useful in scenarios where the input data may be noisy. It can be used to create histograms that describe the distribution of local patterns within an image or a region. These histograms are regularly used as feature-vectors for classification tasks. It is not limited to a specific type of data. It can be applied to various modalities, including images, videos, and 3D data, making it a versatile choice for texture and pattern analysis. By focusing on local neighbourhoods, LBP helps preserve local information, which can be important in tasks where global context is less relevant.

The FetalEcho_V05 dataset framed in the previous research undergoes transformation with two handcrafted image transformation process named as Multispectral Local Binary Pattern (MLBP) and Adaptive Multispectral Local Binary Pattern (AMLBP). These transformations are focusing at better capturing of the minute details in the image leveraging better learning by the models producing classifiers with better and faster diagnostic power. The classifier is further used for classifying the real-time images captured by the device. The overall research framework is depicted in the Fig.2 architecture.

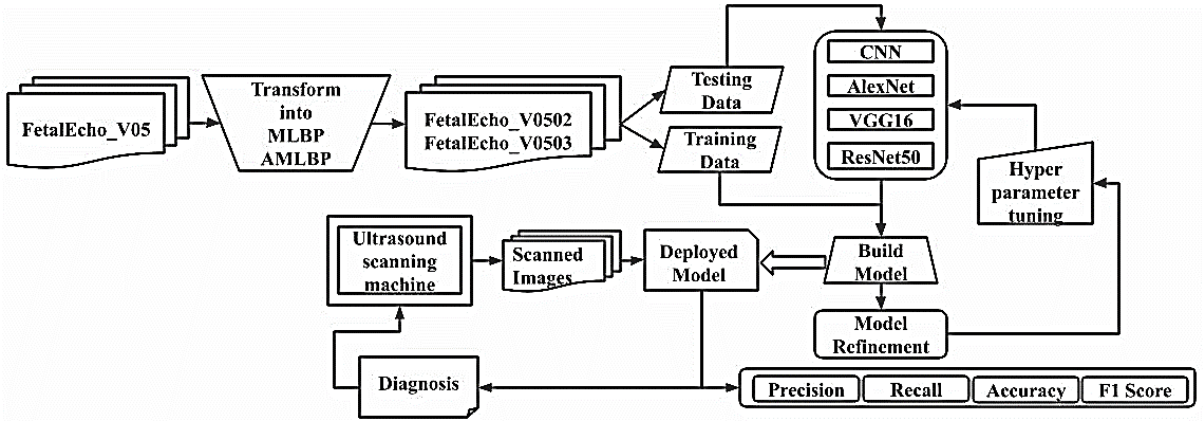

Fig.2 Overall Framework of Fetal Cardiac Anomaly Detection Model

LBP has established itself as a popular method for texture representation in various image processing tasks. It calculates LBP value of one pixel by comparing its gray-level pixel concentration with that of the neighbouring pixels. However, a limitation of LBP is that it is typically computed over grayscale images, thereby overlooking the valuable multi-channel information present in the data. To overcome this drawback of the LBP image transformation can be done by capturing the different colour channel information through the utilization of accumulator patterns and corresponding decoder patterns. This innovative approach enables the incorporation of the multiple channel information into the LBP framework, enhancing its effectiveness and widening its scope in deep learning and classifying applications. Fig.3 shows the process of extracting the multi spectral information from an image.

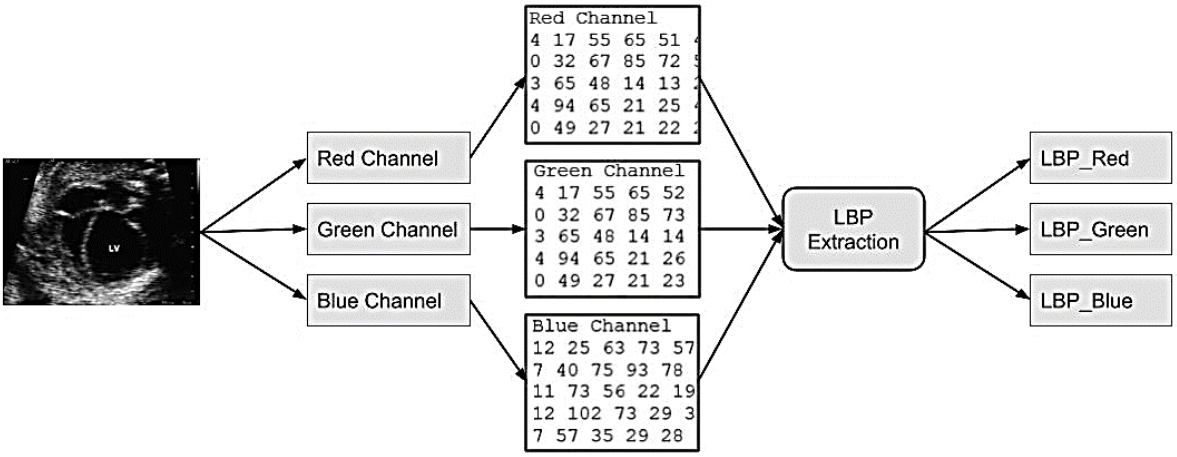

Fig.3 LBP Information retrieval from multiple channels

This research is exploring two different transformation approaches named as Multispectral Local Binary Pattern (MLBP) and Adaptive Multispectral Local Binary Pattern (AMLBP) transformation. The dataset FetalEcho_V05 will be transformed to create FetalEcho_V0502 and FetalEcho_V053 by using MLBP and AMLBP transformations respectively. These datasets are evaluated with the CCNN, Alex Net, VGG16 and Res Net models for classification efficiency of fetal cardiac anomaly classifiers.

4.1 Multispectral Local Binary Pattern (MLBP) Extraction

The MLBP is intended for unfolding the texture of an image. The feature extraction process is described below. Let 'IM' be a multispectral image of size ro * co* ch, where co, ro and ch signify the columns, rows, and channels in numbers correspondingly. Let IM_c be the c[th] channel of the image IM, where, c ∈ [1, ch]. There are J neighbours move apart at equivalent radius from a pixel $IM_c(x,y)$, denoted as $IM_c^j(x,y)$, where i ∈ [1, J], x ∈ [1, ro] and y ∈ [1, co]. The LBP of the present pixel in the present channel c of all channels, $LBP_c(x,y)$, is computed as:

$$LBP_c(x,y) = \sum_{j=1}^{J} LBP_c^n(x,y) \times f^i, \ \ \forall c \in [1, ch] \ \ (1)$$

Where,

$$LBP_c^j(x,y) = \begin{cases} 1, & IM_c^j(x,y) \geq IM_c(x,y) \\ 0, & Otherwise \end{cases} \quad (2)$$

Here, f^j, the weight function used to calculate the decimal equivalent of the resulting LBP is expressed as:

$$f^j = (2)^{(j-1)}, \forall j \in [1, j] \ \ (3)$$

Now, the multispectraladdermap, MLBP(x,y), grounded on these structures is defined as:

$$adder^j(x,y) = \sum_{c=1}^{j} LBP_c^j(x,y) \ (4)$$

The expression "c ∈ [1, ch+1]" indicates that the value of "c" belongs to the interval from 1 to "ch+1". This implies that if the binary pattern of a specific pixel has a value of '1' at a particular position for all channels, then the resulting sum for that pixel, denoted by the variable $adder^j$, will be the sum of the individual channel values.

Once the multispectral adder map is computed, the adder-based LBP, $MLBP_c^n(x,y)$ for the pixel(x,y) of channel 'c' is computed as:

$$MLBP_c^j(x,y) = \begin{cases} 1, & adder^j(x,y) = c-1 \\ 0, & Otherwise \end{cases} \quad (5)$$

For $\forall j \in [1, J] and \ \forall c \in [1, ch+1]$. e

The decimal equivalent of the above pattern can be calculated as:

$$MLBP_c(x,y) = \sum_{j=1}^{J} MLBP_c^j(x,y) \times f^j, \forall c \in [1, ch+1] \quad (6)$$

where f^j is the weight function mentioned in equation (3).

From equations (5) and (6), we can infer that a single pixel of the image will generate ch + 1 patterns. Consequently, this leads to the creation of four output MLBP images. Further a fusion technique is used to combine ch+1 MLBP patterns to create a single and more informative representation. By taking the average value at each pixel location, the fused pattern gives more weight to the most common information from any of the MLBP sources. Fig.2 shows an overall demonstration of one pixel of each LBP of the three colour channels getting converted to MLBP pixel and a sample ultrasound image transformed to MLBP image.

$$MLBP\_Fused(x,y) = AVG(MLBP\_1(x,y), MLBP\_2(x,y), MLBP\_3(x,y), MLBP\_4(x,y) \quad (7)$$

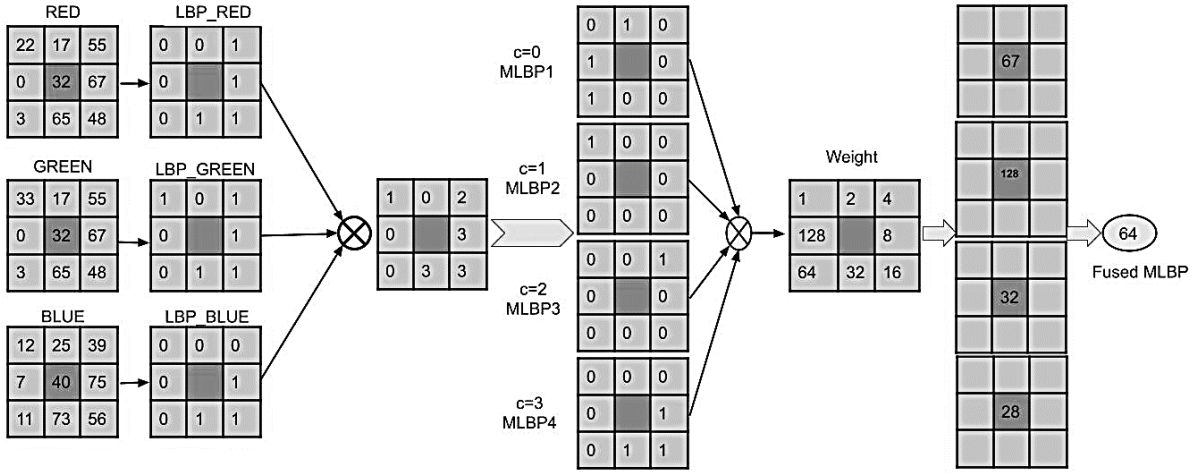

Fig.4. Example of image transformation process using MLBP

Fig.4 shows an sample calculation of MLBP image pixel values. Fig.5 shows a sample fetal echo ultrasound image transformed into an MLBP image using MLBP image transformation technique.

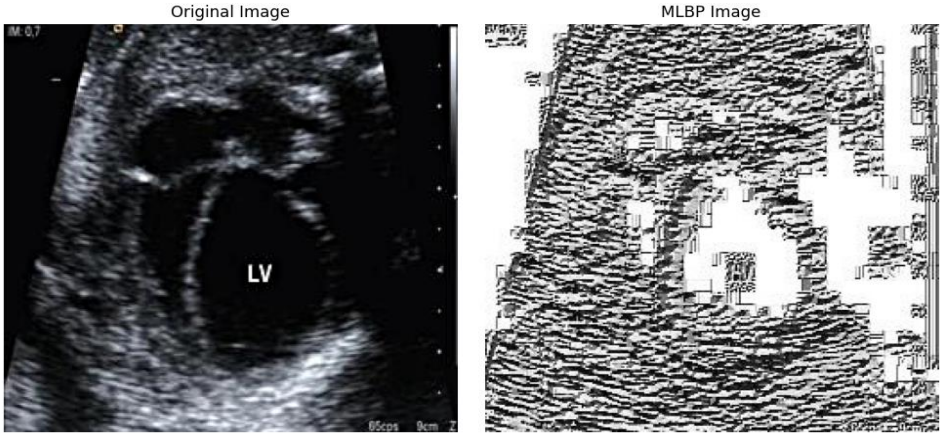

Fig.5 Sample fetal echo ultrasound image after transforming using MLBP technique

4.2 Adaptive Multispectral LocalBinaryPattern (AMLBP) Extraction

The AMLBP stands as an enhanced version of MLBP, utilized for efficiently and simply describing the texture of an image. The feature extraction process is outlined as follows: Let 'IM' denote a multispectral image with dimensions ro × co × ch, where ro, co, and ch represent the number of rows, columns, and channels of the image, respectively. Let IMc denote the c-th channel of the image IM, where c ∈ [1, ch]. It is assumed that there are J neighbors equally spaced at a given radius from any pixel IMc(x,y), denoted as IMc^j(x,y), where j ∈ [1, J], x ∈ [1, ro], and y ∈ [1, co].The LBP of the present pixel in the present channel c of all channels, $LBP_c(x,y)$, is computed with equation (1).

The adder map (AM) is obtained using equation (4). The AMLBP pattern is obtained from the adder map using the below mentioned accumulator truth table Table.1. Resulting eight-bit AMLBP pattern which will be converted into decimal using the weight function f^j.

Table.1 Accumulator

LBP_RED(x,y)	LBP_BLUE(x,y)	LBP_GREEN(x,y)	AM	AMLBP
0	0	0	0	0
1	0	0	1	0
0	1	0	1	0
0	0	1	1	0
1	1	0	2	1
1	0	1	2	1
0	1	1	2	1
1	1	1	3	1

This method when compared to the MLBP transformation take s a smaller number of steps resulting into less execution time and more efficiency by capturing the patterns more efficiently from the images. Fig.3 shows an overall demonstration of one pixel of each LBP of the three colour channels getting converted to MLBP pixel and a sample ultrasound image transformed to MLBP image.'

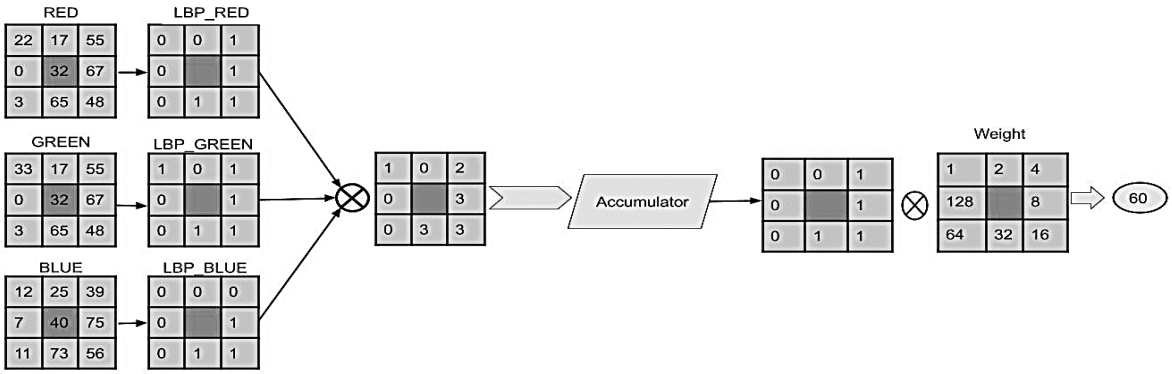

Fig.6 Example of image transformation using AMLBP

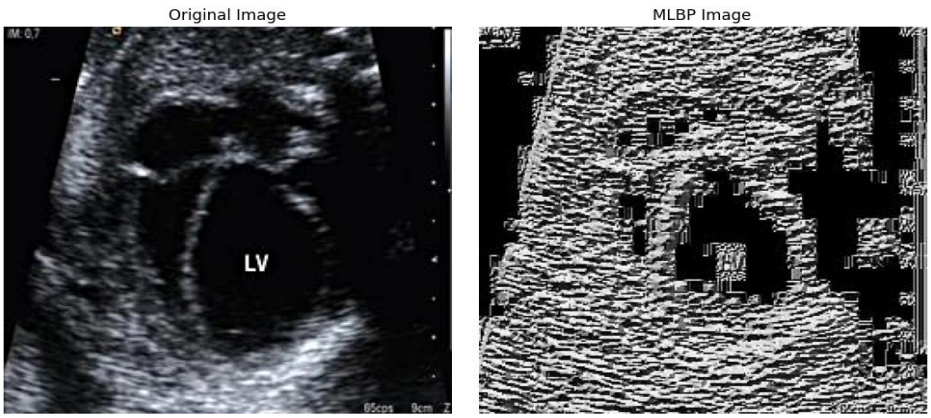

Fig.7 Sample fetal echo ultrasound image after transforming using MLBP technique

Fig.6 shows an sample calculation of AMLBP image pixel values. Fig.7 shows a sample fetal echo ultrasound image transformed into an AMLBP image using MLBP image transformation technique.

The FetalEcho_V0502 obtained after transforming the images using MLBP and FetalEcho_V0503 obtained after transforming the images using AMLBP had undergone experiments with the customized DL models

identified in the previous research. The customized models that were identified in the previous research were CCNN, AlexNet, ResNet50 and VGGNet16.

The FetalEcho_V0502 and FetalEcho_V0503 dataset, comprises of a collection of 1600 images categorized into 16 distinct sets, representing 16 structural heart defects of fetus. Fig.6 (a) and (b) shows some sample images from the dataset FetalEcho_V0502 and FetalEcho_V0503 respectively.

4.3 Model building and Evaluation

In this study, four deep learning (DL) models—AlexNet, CCNN, VGG16, and ResNet50—are employed to analyze the fetal echo dataset. These models are selected based on their consistent performance in prior research [12]. Each model is characterized by specific hyperparameters and customized layers.

The CCNN model is structured as a Sequential model, where layers are stacked sequentially. It starts with a Conv2D layer with 64 filters and a 3x3 kernel size, applying convolutional operations to extract features from input images with ReLU activation for non-linearity. Following this, another Conv2D layer with 32 filters and a 3x3 kernel size refines the extracted features. A Flatten layer converts the 2D feature maps into a 1D vector for fully connected layers. The model includes a Dense layer with 16 units and softmax activation for predicting class probabilities. Stochastic Gradient Descent (SGD) optimizer with a learning rate of 0.001 and categorical cross-entropy loss are utilized for multi-class classification.

AlexNet, renowned for its performance on the ImageNet challenge, begins with a Conv2D layer comprising 96 filters and an 11x11 kernel size, followed by ReLU activation. Max pooling with a 3x3 pool size and a stride of 2x2 reduces feature map dimensions. Successive Conv2D layers follow with 256, 384, and 512 filters, each using ReLU activation and max pooling. The output is flattened and fed into fully connected layers with 4096 units and ReLU activation. Dropout layers with a rate of 0.5 are included to prevent overfitting. The model concludes with a Dense layer featuring softmax activation for multi-class classification. Adam optimizer with a learning rate of 0.001 and categorical cross-entropy loss are employed.

ResNet-50, pre-trained on ImageNet, is fine-tuned for the task with pre-trained layers frozen to retain learned features. A Global Average Pooling 2D layer reduces spatial dimensions, followed by two Dense layers with 1024 units each and ReLU activation to capture high-level patterns. The final Dense layer features softmax activation for multi-class classification. The model uses the Adam optimizer with a learning rate of 0.001 and categorical cross-entropy loss.

Derived from the VGG architecture, the VGG16 model comprises convolutional blocks with escalating filters, followed by max pooling. Fully connected layers handle classification tasks. The first block includes 64 filters with a 3x3 kernel and ReLU activation. Subsequent blocks have 128, 256, 512, and 512 filters. The output is flattened and directed into fully connected layers with 4096 units and ReLU activation. Dropout layers with a rate of 0.5 mitigate overfitting. The final Dense layer with softmax activation facilitates multi-class classification. The model is compiled with categorical cross-entropy loss, Adam optimizer, and accuracy metric.

Each model is trained using 80% of the MLBP images and AMLBP images, and subsequently evaluated using metrics such as precision, recall, accuracy, and F1 score, commonly used for classifier performance assessment.

5. Results and Discussions

Rigorous evaluation of the selected models was carried out using essential metrics such as Accuracy, Precision, Recall, and F1-score on the FetalEcho_V0502 and FetalEcho_V0503 dataset.

For the CCNN model, an 80%/20% train-test split ratio was employed, while for Alex Net, VGG16, and ResNet50, a split ratio of 70%/30% was utilized. The learning rates were set at 0.001 for CCNN and 0.0001 for Alex Net, VGG16, and ResNet50. Regarding optimization algorithms, Stochastic Gradient Descent (SGD) was used for CCNN, Local Response Normalization for Alex Net, Momentum SGD for VGG16, and Adaptive Moment Estimation for ResNet50. The ReLU activation function was chosen for all models during training, and the loss functions applied were Softmax Cross-Entropy for CCNN and Categorical Cross-Entropy for AlexNet, VGG16, and ResNet50.

Each model featured varying numbers of hidden layers, with CCNN having 10, Alex Net with 40, VGG16 with 50, and ResNet50 with 10. To combat overfitting, dropout with rates of 0.5 was applied for CCNN, 0.4 for Alex Net and VGG16, and 0.3 for ResNet50. In each training epoch, the models underwent 20 iterations, and kernel filter sizes were set to 3x3 for CCNN, 11x11 for AlexNet, and 3x3 for VGG16 and ResNet50. Max-pooling was chosen as the pooling technique, and a batch size of 64 was used, along with 100 epochs to ensure adequate model training. Table.2 shows the hyperparameter setting for all the four models.

Table 2. Hyper parameters settings

Models	Train-test split ratio	Learning rate	Optimization algorithm	Activation function	Loss function	Number of hidden layers	The drop-out rate	Number of iterations per epoch	Kernel or filter size in convolutional layers	Poling-ng size	Batch size	Ep-och
CCNN	0.8-0.2	0.001	Stochastic Gradient Descent (SGD)	ReLU	Softmax Cross-Entropy	10	0.5	20	3*3	Max-pooling	64	100
AlexNet	0.7-0.3	0.0001	Local Response Normalization	ReLU	Categorical cross entropy	40	0.4	20	11*11	Max-pooling	64	100
VGG16	0.7-0.3	0.0001	Momentum SGD	ReLU	Categorical cross entropy	50	0.4	20	3*3	Max-pooling	64	100
ResNet 50	0.7-0.3	0.0001	Adaptive Moment Estimation	ReLU	Categorical cross entropy	10	0.3	20	3*3	Max-pooling	64	100

After extensive iterations and thorough hyperparameter tuning, the CCNN model appeared as the top-performing classifier for the MLBP image dataset, FetalEcho_V0502. It delivered impressive results with precision, accuracy, recall, and F1 scores of 0.94, 0.92, 0.94, and 0.93, respectively. In contrast, the AlexNet model achieved precision, accuracy, recall, and F1 scores of 0.92, 0.89, 0.89, and 0.89, respectively. Similarly, the VGG16 model demonstrated notable performance, yielding precision, accuracy, recall, and F1 scores of 0.91, 0.87, 0.89, and 0.88, respectively. Additionally, the ResNet50 model attained precision, accuracy, recall, and F1 score of 0.93, 0.92, 0.93, and 0.93, respectively. Upon comprehensive evaluation, the CCNN model exhibited superior predictive capabilities compared to the other models on the FetalEcho_V0501 dataset. Tables 3 and 4 present the performance evaluation of the MLBP classifier and AMLBP classifier, respectively, illustrating the precision, accuracy, recall, and F1 scores for each model.

Table.3 Performance Results of Image Classification Models based on MLBP image dataset - FetalEcho_V0502

Models	Precision	Recall	Accuracy	F1 Score
CCNN	0.94	0.92	0.94	0.93
VGG16	0.91	0.88	0.89	0.88
AlexNet	0.92	0.89	0.89	0.89
ResNet50	0.93	0.92	0.93	0.93

After multiple iterations, the CCNN model was identified as the optimal model for the AMLBP image dataset, FetalEcho_V0503. recall, For the AlexNet model, the metrics were precision of 0.92, recall of 0.90, accuracy of 0.91, and F1 score of 0.90. Similarly, the VGG16 model achieved a precision - 0.92, recall - 0.90, accuracy - 0.91, and F1 score - 0.89. Lastly, the ResNet50 model yielded precision, recall, accuracy, and F1 score of 0.94, 0.93, 0.94, and 0.93, respectively. Considering the overall performance, the CCNN model emerged as the top performer on the FetalEcho_V0502 dataset. The detailed results are presented in Table 3, outlining the precision, recall, accuracy, and F1 scores for each model.

Table.4. Performance Results of Image Classification Models based on AMLBP image dataset - FetalEcho_V0503

Models	**Precision**	**Recall**	**Accuracy**	**F1 Score**
CCNN	0.95	0.93	0.94	0.93
VGG16	0.92	0.90	0.91	0.89
AlexNet	0.92	0.90	0.91	0.90
ResNet50	0.94	0.93	0.94	0.93

After conducting multiple iterations, it was found that the CCNN model outperformed other models on the FetalEcho_V0501 dataset. It achieved notable precision, accuracy, recall, and F1 score of 0.95, 0.94, 0.93, and 0.93, respectively. AlexNet exhibited precision, accuracy, recall, and F1 score of 0.92, 0.91, 0.90, and 0.90, while the VGG16 model achieved a precision of 0.92, recall of 0.90, accuracy of 0.91, and F1 score of 0.89. The ResNet50 model yielded precision, recall, accuracy, and F1 score of 0.94, 0.93, 0.934, and 0.93, respectively. Overall, CCNN demonstrated superior performance on the FetalEcho_V0501 dataset. These results are summarized in Table 4, providing details on precision, recall, accuracy, and F1 scores for each model.

In prior research, LBP transformations were utilized to construct the FetalEcho_V0501 dataset, focusing on fetal cardiac anomaly detection. The CCNN model achieved precision, accuracy, recall, and F1 score of 0.94, 0.93, 0.91, and 0.93, respectively. AlexNet showed precision, accuracy, recall, and F1 score of 0.92, 0.89, 0.88, and 0.89, while the VGG16 model attained precision, accuracy, recall, and F1 score of 0.91, 0.87, 0.87, and 0.89, respectively. Lastly, the ResNet50 model yielded precision, accuracy, recall, and F1 score of 0.93, 0.93, 0.91, and 0.93, respectively. CCNN emerged as the best performer on the FetalEcho_V0501 dataset. These previously obtained results are reconfirmed in Table 5, illustrating precision, recall, accuracy, and F1 scores for each model.

Table 5. Performance Results of Image Classification Models based on LBP image dataset - FetalEcho_V0501

Models	Precision	Recall	Accuracy	F1 Score
CCNN	0.94	0.91	0.93	0.93
VGG16	0.91	0.87	0.87	0.89
AlexNet	0.92	0.88	0.89	0.89
ResNet50	0.93	0.91	0.93	0.93

Comparative Analysis

The performance results for the DL classifiers for the three transformation techniques LBP, MLBP and AMLBP are recorded using the precision, accuracy recall, and F1-score metrics. The values are depicted in the table. Foe easy comparison the Fig.8 shows the chart illustrating the performance of the three transformation techniques.

Table 6. The result illustration of all three transformation techniques

Transformation Technique	Models	Precision	Recall	Accuracy	F1 Score
LBP	CCNN	0.94	0.91	0.93	0.93
	AlexNet	0.92	0.88	0.89	0.89
	VGG16	0.91	0.87	0.87	0.89
	ResNet50	0.93	0.91	0.93	0.93
MLBP	CCNN	0.94	0.92	0.94	0.93
	AlexNet	0.92	0.89	0.89	0.89
	VGG16	0.91	0.88	0.89	0.88
	ResNet50	0.93	0.92	0.93	0.93
AMLBP	CCNN	0.95	0.93	0.94	0.93
	VGG16	0.92	0.9	0.91	0.89
	AlexNet	0.92	0.9	0.91	0.9
	ResNet50	0.94	0.93	0.94	0.93

The charts below Fig.8, Fig.9, Fig.10, and Fig.11 visualise a clear comparison between the four performance evaluation metrics for different transformation techniques and the model combination.

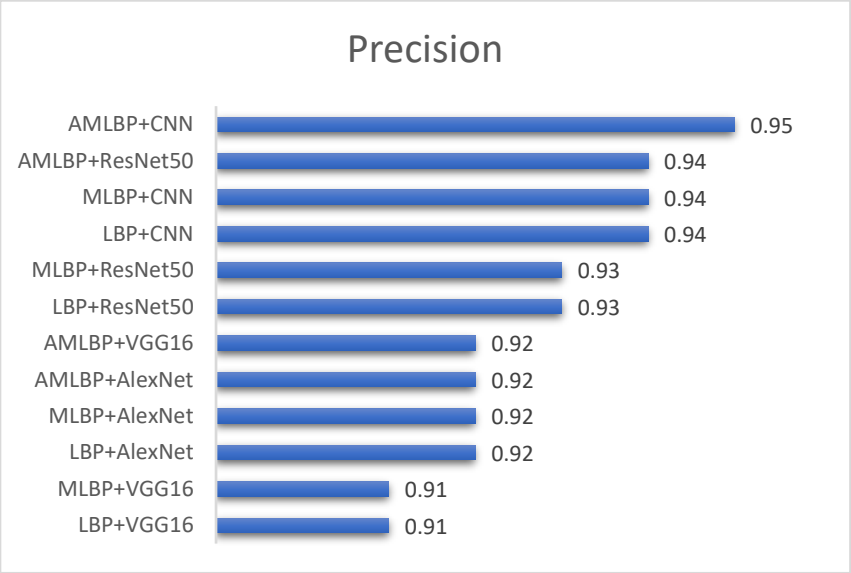

Fig.8. Precision values obtained for all the transformation technique and model combination

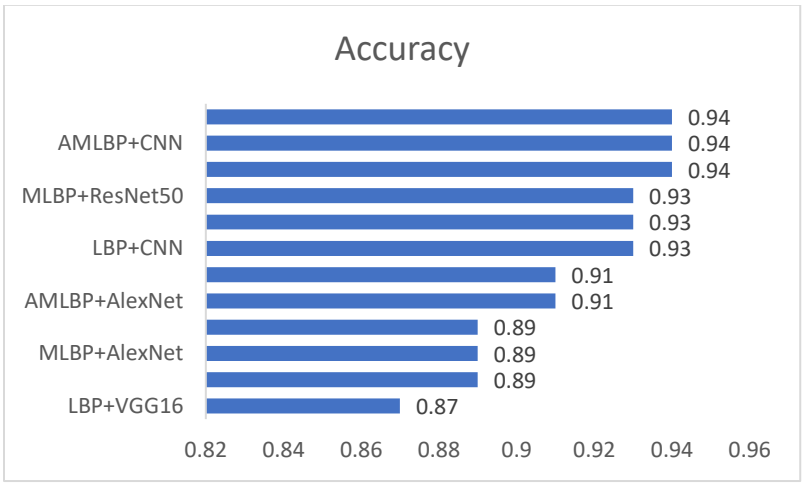

Fig.9. Accuracy values obtained for all the transformation technique and model combination

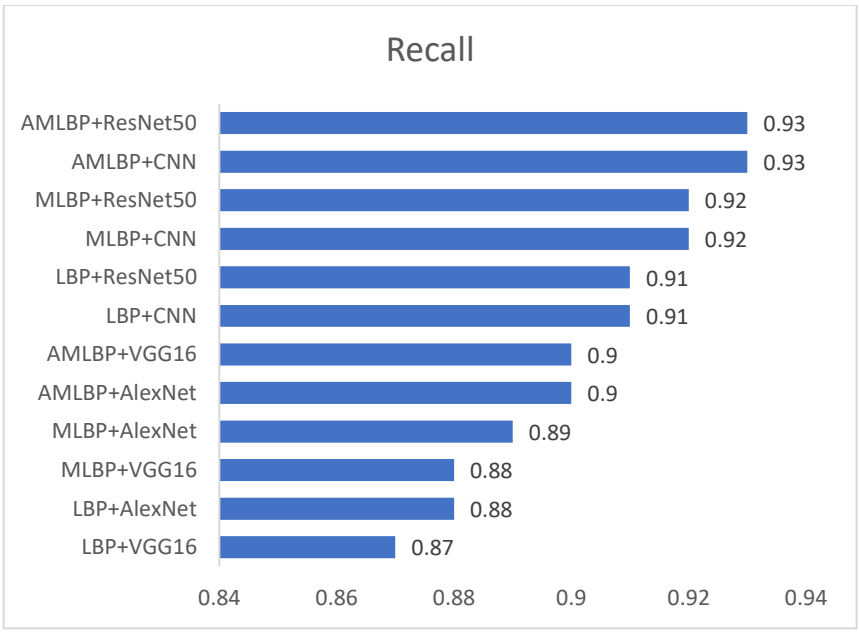

Fig.10. Recall values obtained for all the transformation technique and model combination

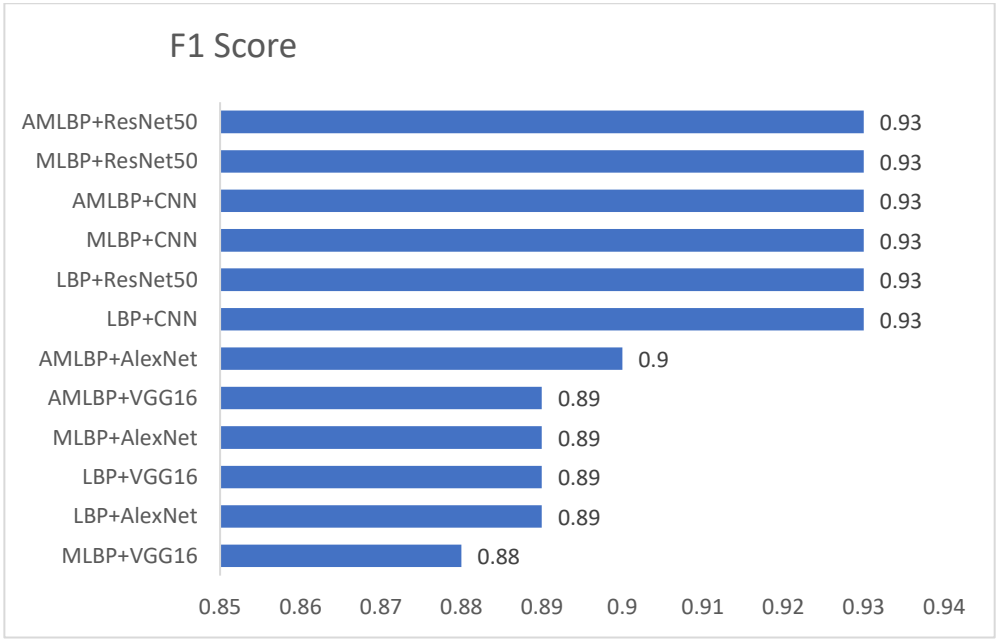

Fig.11. Precision values obtained for all the transformation technique and model combination

When the performance of the DL models on FetalEcho_V0502 and FetalEcho_V0503 datasets is analysed, FetalEcho_V0501 and FetalEcho_V0502 datasets, the CCNN model proved to be the best-performing classifier in both cases. On the FetalEcho_V0501 dataset, the CCNN model achieved impressive precision, accuracy, recall, and F1 scores of 0.94, 0.93, 0.91, and 0.93, respectively. Similarly, on the FetalEcho_V0502 dataset, the CCNN model exhibited outstanding results with precision, accuracy, recall, and F1 scores of 0.94, 0.934, 0.92, and 0.93, respectively.

On the other hand, the AlexNet model delivered competitive results in both datasets, with precision, accuracy, recall, and F1 scores of 0.92, 0.89, 0.88, and 0.89 on the FetalEcho_V0501 dataset, and 0.92, 0.89, 0.89, and 0.89 on the FetalEcho_V0502 dataset.

The VGG16 model also demonstrated notable performance in both datasets, achieving precision, accuracy, recall, and F1 scores of 0.91, 0.87, 0.87, and 0.89 on the FetalEcho_V0501 dataset, and 0.91, 0.88, 0.89, and 0.88 on the FetalEcho_V0502 dataset.

Lastly, the ResNet50 model showcased consistent and robust results in both datasets, with precision, accuracy, recall, and F1 scores of 0.93, 0.93, 0.91, and 0.93 on the FetalEcho_V0501 dataset, and 0.93, 0.92, 0.93, and 0.93 on the FetalEcho_V0502 dataset.

Overall, the CCNN model stood out as the most effective classifier for fetal echo USIT image classification, demonstrating superior predictive capabilities in both datasets. These findings highlight the CCNN model's versatility and reliability in diagnosing fetal cardiac anomalies across different datasets, making it a compelling choice for real-world applications. The summarized results are presented in Table.3 for MLBP transformation (FetalEcho_V0502) and Table.4 for AMLBP transformation (FetalEcho_V0503), reaffirming the CCNN model's superiority in fetal echo USIT image classification for enhanced fetal cardiac anomaly diagnosis.

Findings

The transformation techniques MLBP and AMLBP showed improvement for all the four classifiers and amongst the two, AMLBP transformation produced best and consistent results for all the performance metrics and the classifiers are taken into consideration. The overall performance of the MLBP transformation technique, the CCNN model stood out as the most effective and robust classifier, excelling in accurately detecting fetal cardiac anomalies. While applying AMLBP transformation, CCNN classifier found as the best performing. As per the results, the ResNet50 model is the second-best performing classifier for the MLBP transformation technique and for AMLBP transformation also ResNet is at par with the CCNN classifier where only a 1% difference in Precision had put it to the second position. The VGG16 and AlexNet classifiers achieved commendable improvement in precision, recall, accuracy, and F1 scores for both the transformation techniques. The previous research had checked the LBP transformed version of the dataset. The performance of MLBP and AMLBP is overruling the LBP transformation process. Through rigorous evaluation, the best hyperparameter configurations also identified that yield the highest classifier performance. The CCNN classifier emerged as the top-performing model, closely followed by the ResNet50 classifier, exhibiting a marginal variance in performance.

6. Conclusion

The study delved into the utilization of Multispectral Local Binary Patterns (MLBP) and Adaptive Multispectral Local Binary Patterns (AMLBP) transformations on images to create new datasets, namely FetalEcho_V0502 and FetalEcho_V0503. Prior to experimentation, the pre-processed datasets underwent essential standardization and normalization procedures. Employing tailored DL architectures, including AlexNet, CCNN, VGG16, and ResNet50, the research proceeded to train these models using the transformed datasets, employing thoughtfully chosen hyperparameters to construct effective classifiers.

Through meticulous evaluation employing precision, accuracy, recall, and F1-score metrics, the performance of these classifiers was rigorously assessed, and the results were comprehensively documented. The empirical findings unequivocally highlight notable enhancements in classifier performance when trained on the MLBP (FetalEcho_V0502) and AMLBP (FetalEcho_V0503) image datasets. By capitalizing on advanced image transformation methodologies, coupled with sophisticated deep learning approaches and a robust assessment framework, this study contributes to the progress of fetal cardiac anomaly detection.

References

[1] Patil, V. K., et al. ‘Real Time Emotion Recognition with AD8232 ECG Sensor for Classwise Performance Evaluation of Machine Learning Methods’. International Journal of Engineering, vol. 36, no. 6, 2023, pp. 1040–1047.

[2] Khazendar, S., et al. ‘Automated Characterisation of Ultrasound Images of Ovarian Tumours: The Diagnostic Accuracy of a Support Vector Machine and Image Processing with a LocalBinaryPattern

Operator'. Facts, Views & Vision in ObGyn, vol. 7, 2015.

[3] Zeebaree, D. Q., et al. 'Multi-Level Fusion in Ultrasound for Cancer Detection Based on Uniform LBP Features'. Uniform LBP Features. Computers, Materials & Continua, no. 3, 2021.

[4] Iakovidis, Dimitris K., et al. 'Fuzzy Local Binary Patterns for Ultrasound Texture Characterization'. Lecture Notes in Computer Science, Springer Berlin Heidelberg, 2008, pp. 750–759, https://doi.org10.1007/978-3-540-69812-8_74. Lecture Notes in Computer Science.

[5] Liu, Tianjiao, et al. 'Classification of Thyroid Nodules in Ultrasound Images Using Deep Model Based Transfer Learning and Hybrid Features'. 2017 IEEE International Conference on Acoustics, Speech and Signal Processing (ICASSP), IEEE, 2017, https://doi.org10.1109/icassp.2017.7952290.

[6] Divya, M. O., and M. S. Vijaya. 'Artificial Intelligent Models for Automatic Diagnosis of Foetal Cardiac Anomalies: A Meta-Analysis'. Proceedings of the International Conference on Cognitive and Intelligent Computing, Springer Nature Singapore, 2023, pp. 179–192, https://doi.org10.1007/978-981-19-2358-6_18.

[7] Divya, M. O., and M. S. Vijaya. "Optimizing Pre-processing for Foetal Cardiac Ultra Sound Image Classification." International Conference on Innovations in Bio-Inspired Computing and Applications. Cham: Springer Nature Switzerland, 2022.

[8] Divya, M. O., and E. R. Vimina. 'Content Based Image Retrieval with Multi-Channel LBP and Colour Features'. International Journal of Applied Pattern Recognition, vol. 6, no. 2, Inderscience Publishers, 2020, p. 177, https://doi.org10. 1504/ijapr.2020.111524.

[9] Vimina, E. R., and M. O. Divya. 'Maximal Multi-Channel Local Binary Pattern with Colour Information for CBIR'. Multimedia Tools and Applications, vol. 79, 2020, pp. 25357–25377.

[10] 'Diagnostic Models for Foetal Cardiac Anomalies Using Pattern Classification and FetalEcho_V01 Dataset (In Press)'. Proceedings of the Eighth International Conference on Computing, Communication and Security (ICCCS 2023, 2023.

[11] MO, DIVYA, and M. S. Vijaya. "REVOLUTIONIZING FOETAL CARDIAC ANOMALY DIAGNOSIS: UNLEASHING THE POWER OF DEEP LEARNING ON FOETALECHO IMAGES." Journal of Theoretical and Applied Information Technology 101.16 (2023).

[12] Holland, B. J., et al. 'Prenatal Diagnosis of Critical Congenital Heart Disease Reduces Risk of Death from Cardiovascular Compromise Prior to Planned Neonatal Cardiac Surgery: A Meta-Analysis'. Ultrasound in Obstetrics & Gynecology: The Official Journal of the International Society of Ultrasound in Obstetrics and Gynecology, vol. 45, no. 6, Wiley, June 2015, pp. 631–638, https://doi.org10.1002/uog.14882.

[13] Suard, Cornélie, et al. 'Accuracy of Prenatal Screening for Congenital Heart Disease in Population: A Retrospective Study in Southern France'. PloS One, vol. 15, no. 10, Public Library of Science (PLoS), Oct. 2020, p. e0239476, https://doi.org10.1371/journal.pone.0239476.

[14] Changlani, Trupti Deepak, et al. 'Outcomes of Infants with Prenatally Diagnosed Congenital Heart Disease Delivered in a Tertiary-Care Pediatric Cardiac Facility'. Indian Pediatrics, vol. 52, no. 10, Springer Science and Business Media LLC, Oct. 2015, pp. 852–856, https://doi.org10.1007/s13312-015-0731-x.

[15] Vijayaraghavan, Aparna, et al. 'Prenatal Diagnosis and Planned Peri-Partum Care as a Strategy to Improve Pre-Operative Status in Neonates with Critical CHDs in Low-Resource Settings: A Prospective Study'. Cardiology in the Young, vol. 29, no. 12, Cambridge University Press (CUP), Dec. 2019, pp. 1481–1488, https://doi.org10.1 017/S104 795111900252X.